Published in IET Electric Power Applications
Received on 19th July 2013
Revised on 6th December 2013
Accepted on 27th December 2013
doi: 10.1049/iet-epa.2013.0248

ISSN 1751-8660

Decoupled control for integrated rotary–linear switched reluctance motor

Jianfei Pan, Fanjie Meng, Guangzhong Cao

Shenzhen Key Laboratory of Electromagnetic Control, College of Mechatronics and Control Engineering, Shenzhen University, Shenzhen, Guangdong Province, People's Republic of China
E-mail: cao_guangzhong@163.com

Abstract: The integrated direct-drive rotary–linear switched reluctance motor (RLSRM) is investigated in this paper. The characteristics of the RLSRM are further inspected by using the finite element method after theoretical analysis. The torque and force distribution function (TFDF) is proposed for the RLSRM based on the multiphase excitation scheme to decouple the linear and the rotary axis of motion. Based on the simple proportional–integral-derivative position control algorithm, the experimental results testify the effectiveness of the proposed TFDF for individual control for each axis.

1 Introduction

In modern industry, high-precision position control of two degree-of-freedom motions for simultaneous rotary and linear movement is in high demand, such as printed circuit board drilling, laser soldering and component packaging and so on. Traditionally, these kinds of motions are commonly realised by two separate motors stacked on top of each other, coupled with necessary mechanical rotary-to-linear translators. However, it often leads to a complexity in the mechanical structure, bulk in volume, slow response and low-precision positioning problems. Drive-drive rotary–linear motors, capable of torque and axial force generation at the same time, have aroused researchers' attention [1].

The direct-drive machine has the characteristics of a simplified mechanical structure, improved dynamic performance and adaptation to certain working environments [2–7]. Krebs *et al.* [2] proposed an integrated permanent magnet (PM) rotary-linear machine with an iron toothed armature and a concentrated coil structure. The machine applies 48 alternatively polarised PMs for the mover and the stator has 18 salient poles with coils. The design and the modelling of the PM rotary–linear motor for different operating points are discussed in [3] and a decoupling control method based on the $d-q$ transformation is studied in [4]. Based on the PM machine principle, a rotary–linear motor with less complexity dedicated to electric vehicle wheels has been discussed [5, 6]. The synchronous machine applies two stators with windings and one mover core with PMs for a three-phase flux circulation. Aiming at Joule losses minimisation, an optimisation process is developed based on the analytical study [7].

The rotary-linear motors discussed above require PMs to facilitate a magnetic flux circulation. The involvement of the PMs often leads to high production and assembly cost, even a complicated winding structure. Furthermore, the overall control system is complex and expensive. The switched reluctance motor (SRM) is an attractive solution because of its remarkable advantages such as simple and robust construction, low cost and the capability of withstanding hostile environments [8].

Two kinds of integrated rotary–linear SRMs have been proposed in [9–11]. The first type utilises a pair of rotary stator windings and three linear propulsion windings that correspond to a typical '6/4' linear SRM [9, 10]. The mover poles are alternatively toothed on the shaft. This kind of machine is capable of a long stroke movement. The structure of the three stator phases for the integrated rotary and linear movement with a multi-segmented structure based on the simulation analysis is proposed in [11]. Although it can realise a long distance movement, the modular cascaded stators lead to a complex winding structure and drive topology. In [12], the rotary–linear SRM with one rotary stator and two linear propulsion stators for a short-distance stroke operation is introduced. To further minimise the number of the stators, a machine with double identical stators for both rotary and linear motion is proposed [13]. The output force and the torque can be independently controlled based on the proportional–integral-derivative (PID) algorithm. For angular and linear position detection, the control system applies three reflective fibre optic switches for shaft angle detection and a conductive plastic potentiometer for linear position sensing. Therefore the sensing system is complicated since the optic switches must be mounted on the stator poles inside the machine housing. Furthermore, the rotary and the linear axes of the movement are highly coupled and a proper decoupling algorithm should be developed for the integrated rotary-linear machine.

The current research mainly focuses on the design and the optimisation of the rotary–linear switched reluctance motors

(RLSMs) and a high-precision position control performance has not yet been realised because of the high coupling features between the axes of the motions. To obtain a better operation performance, this paper proposes a decoupling motion control algorithm based on a novel torque and force distribution function (TFDF). Apart from the previous paper discussed above, the proposed torque and the force function are capable of independent and simultaneous position control for each axis of motion. The proposed function and the control method are verified by simulation and experiment on the RLSRM. Both the simulation and the experimental results indicate that the proposed motion control system implemented with the decoupling algorithm can achieve a certain control precision for each axis of motion. The system also exhibits a certain load disturbance rejection capability.

After a thorough investigation of the coupling characteristics of the rotary and the linear motion for the RLSRM in Section 2, the TFDF that aims to decouple the two axes of motion is proposed for an independent control of the rotary and the linear axis simultaneously in Section 3. In Section 4, the simple yet effective PID algorithm is employed for an independent control of both the axes of motion. Section 5 provides the experimental results that validate the effectiveness of the proposed TFDF.

2 Machine structure and modelling

2.1 Machine structure of the RLSRM

Fig. 1*a* shows the primary structure of the RLSRM, which mainly consists of stator I, stator II and the mover with a shaft. The stators are identical and each stator has a set of three-phase windings. The stators are located on the base at a zero phase shift. The topology of each stator and the mover corresponds to a typical '6/4' SRM. A pair of rotary–linear bearings are installed coaxially to facilitate the shaft for rotary and linear movement at the same time. Since the shaft is not locked and supported by the brackets with integrated bearings, linear motion in two directions of the x-axis can be performed by a proper excitation of the phases(s) from the two stators. Instead of the fibre optic switches for angular displacement detection, a rotary optical encoder is installed on the fixture and it is concentrical with the shaft. The fixture also integrates a linear magnetic encoder for translational position measurement. The damper protects the fixture from hitting the bracket if a large linear motion overshoot is expected. Compared with the previously constructed rotary–linear machine [13], the rotary and the linear encoders can be independently installed. The following advantages of the machine can be summarised:

1. least winding arrangement and a simple winding scheme with the coils mounted on the stator with an adjustable linear stroke,
2. simple and robust machine structure,
3. low overall production cost,
4. good heat dissipation with an open machine structure,
5. capable of operation under an extreme environment if the encoders are kept outside.

Fig. 1*b* shows the overall structure of the RLSRM prototype and the major machine specifications are tabulated in Table 1.

2.2 Modelling of the RLSRM

The RLSRM can be regarded as a typical mechatronic system according to the principle of energy conservation as [14]

$$dW_{\mathrm{e}} = dW_{\mathrm{l}} + dW_{\mathrm{s}} + dW_{\mathrm{m}} \tag{1}$$

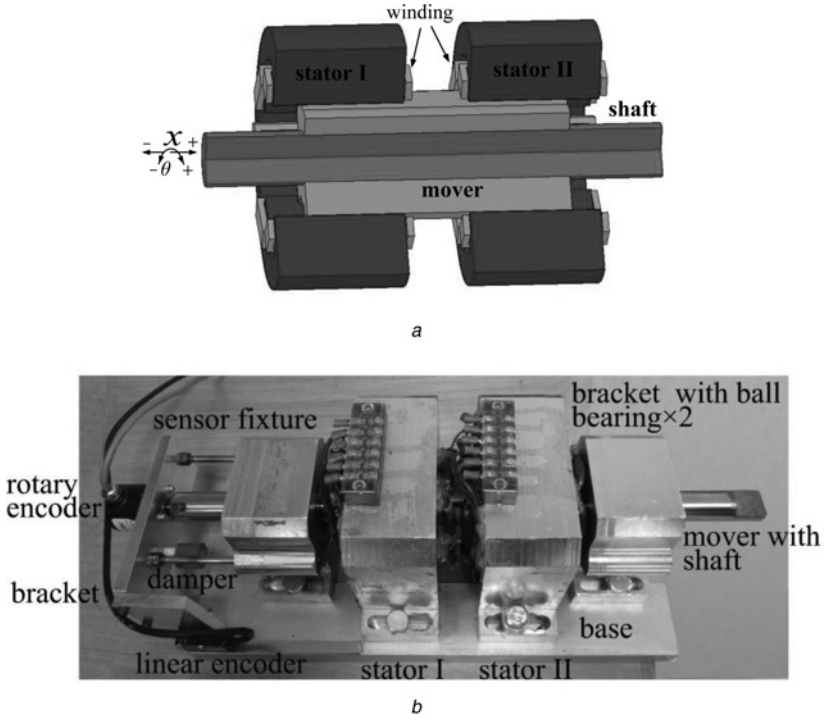

Fig. 1 *Structure of the RLSRM*

a Machine structure
b Prototype

doi: 10.1049/iet-epa.2013.0248

Table 1 Major machine specifications

Parameter	Value
material model	50W1300
lamination thickness	0.5 mm
air gap length	0.5 mm
mover mass	3.35 kg
no. of turns per phase	150
phase conductivity	2×10^6 s/m
stator arc length	40°
rotor arc length	40°
slot arc length	20°
pole-pitch (rotary axis)	60°
phase resistance	7.8 Ω

where dW_e, dW_l, dW_s and dW_m are the incremental electric input energy, the incremental loss energy dissipated by heat, the incremental stored magnetic energy and the incremental mechanical energy, respectively. For the linear axis of movement, the incremental mechanical energy in terms of the propulsion force and a change in the mover position can be represented as

$$dW_{mx} = F_x dx \tag{2}$$

where F_x is the propulsion force and dx is the incremental linear displacement from the mover in the axial direction. For the rotary axis of motion, the incremental mechanical energy in terms of an electromagnetic torque and a change in the rotor position can be expressed as

$$dW_{m\theta} = T_\theta d\theta \tag{3}$$

where T_θ is the electromagnetic torque and $d\theta$ is the incremental angular displacement. In the case of the RLSRM, the incremental mechanical energy can be expressed as

$$dW_m = F_x dx + T_\theta d\theta \tag{4}$$

The dynamic model of the RLSRM in the rotary and the linear directions can be reconstructed as follows

$$\begin{cases} F_x = M\ddot{x} + D\dot{x} + f \\ T_e = J\ddot{\theta} + K\dot{\theta} + T_{\mathrm{L}} \end{cases} \tag{5}$$

where M, D and f are the masses of the mover, the friction coefficient and the load force. J is the moment of inertia, K is the friction coefficient and T_{L} is the load torque.

By neglecting the mutual inductance between the phases, the voltage balancing equation can be characterised as [14]

$$u = Ri + \frac{\mathrm{d}\Psi(\theta, x, i)}{\mathrm{d}t} \tag{6}$$

where R is the resistance and the flux-linkage and Ψ is the function of the angle, the mover position and the phase current, respectively. In the linear region, it can be further expressed as

$$\Psi = L(\theta, x, i)i \tag{7}$$

where L is the inductance dependent on the angle, the mover position and the phase current. Equation (6) can be rewritten as (see (8))

In (8), it shows that the phase voltage is equal to the sum of the resistive voltage drop given by Ri, the induced voltage drop $(L(\theta, x, i) + i(\mathrm{d}L(\theta, x, i)/\mathrm{d}i))\ (\mathrm{d}i/\mathrm{d}t)$ and the back electromotive force, identified by the term $i(\mathrm{d}L(\theta, x, i)/\mathrm{d}\theta)\ \omega_m + i(\mathrm{d}L(\theta, x, i)/\mathrm{d}x)v_x$. ω_m is the angular speed and v_x is the linear motion speed. The electromagnetic force F_x and the torque T_θ in the linear region can be represented as

$$\begin{cases} F_x = \dfrac{1}{2} i^2 \dfrac{\mathrm{d}L(\theta, x, i)}{\mathrm{d}x} \\ T_\theta = \dfrac{1}{2} i^2 \dfrac{\mathrm{d}L(\theta, x, i)}{\mathrm{d}\theta} \end{cases} \tag{9}$$

Both the two stators, have a set of three-phase windings. As the three phases are considered, the voltage balancing equation can be represented in the matrix form as

$$\boldsymbol{U} = \boldsymbol{RI} + \frac{\mathrm{d}}{\mathrm{d}t}\boldsymbol{\psi} \tag{10}$$

where $\boldsymbol{U} = [U_A, U_B, U_C]^{\mathrm{T}}$, $\boldsymbol{R} = \mathrm{diag}[R_A, R_B, R_C]$, $\boldsymbol{I} = [i_A, i_B, i_C]^{\mathrm{T}}$ and $\boldsymbol{\psi} = [\psi_A, \psi_B, \psi_C]^{\mathrm{T}}$, respectively, with

$$\begin{bmatrix} \psi_A \\ \psi_B \\ \psi_C \end{bmatrix} = \begin{bmatrix} L_{AA} & L_{AB} & L_{AC} \\ L_{BA} & L_{BB} & L_{BC} \\ L_{CA} & L_{CB} & L_{CC} \end{bmatrix} \begin{bmatrix} i_A \\ i_B \\ i_C \end{bmatrix} \tag{11}$$

If $i = j$, then L_{ij} stands for the self-inductance of the ith phase; otherwise, it is the mutual inductance from another phase, which is expressed as a function of the rotary displacement, the linear displacement and the current, respectively. The electromagnetic torque T_θ and the propulsion force F_x can thus be rewritten as

$$\begin{cases} F_x = \dfrac{1}{2} I^{\mathrm{T}} \left(\dfrac{\partial}{\partial x} L \right) I \\ \mathrm{T}_\theta = \dfrac{1}{2} I^{\mathrm{T}} \left(\dfrac{\partial}{\partial \theta} L \right) I \end{cases} \tag{12}$$

The partial derivatives of the inductance with respect to the linear and the angular position are denoted as g_θ and g_x, respectively. The change of the inductance from the linear

$$\begin{aligned} u &= Ri + \frac{\mathrm{d}\{L(\theta, x, i)i\}}{\mathrm{d}t} \\ &= Ri + L(\theta, x, i)\frac{\mathrm{d}i}{\mathrm{d}t} + i\frac{\mathrm{d}L(\theta, x, i)}{\mathrm{d}\theta}\frac{\mathrm{d}\theta}{\mathrm{d}t} + i\frac{\mathrm{d}L(\theta, x, i)}{\mathrm{d}x}\frac{\mathrm{d}x}{\mathrm{d}t} + i\frac{\mathrm{d}L(\theta, x, i)}{\mathrm{d}i}\frac{\mathrm{d}i}{\mathrm{d}t} \\ &= Ri + \left(L(\theta, x, i) + i\frac{\mathrm{d}L(\theta, x, i)}{\mathrm{d}i} \right)\frac{\mathrm{d}i}{\mathrm{d}t} + i\frac{\mathrm{d}L(\theta, x, i)}{\mathrm{d}\theta}\omega_m + i\frac{\mathrm{d}L(\theta, x, i)}{\mathrm{d}x}v_x \end{aligned} \tag{8}$$

and the rotary axes of motion can be described as

$$\frac{\partial}{\partial x}L = \begin{bmatrix} g_{xAA} & g_{xAB} & g_{xAC} \\ g_{xAB} & g_{xBB} & g_{xBC} \\ g_{xAC} & g_{xBC} & g_{xCC} \end{bmatrix} \tag{13}$$

$$\frac{\partial}{\partial \theta}L = \begin{bmatrix} g_{\theta AA} & g_{\theta AB} & g_{\theta AC} \\ g_{\theta AB} & g_{\theta BB} & g_{\theta BC} \\ g_{\theta AC} & g_{\theta BC} & g_{\theta CC} \end{bmatrix} \tag{14}$$

3 Torque and force distribution function

3.1 Current derivation

Owing to the large air gap region between the mover and the stators, the torque and the force can be considered under a full operation of the linear region. From (9), the force and the torque generation for the stators I and II can be rewritten as

$$\begin{cases} F_x^{\mathrm{I}} = \dfrac{1}{2} i_m^2 \dfrac{\mathrm{d}L(\theta, x, i_m)}{\mathrm{d}x} = \dfrac{1}{2} i_m^2 g_{xm}^{\mathrm{I}} \\ T_\theta^{\mathrm{I}} = \dfrac{1}{2} i_m^2 \dfrac{\mathrm{d}L(\theta, x, i_m)}{\mathrm{d}\theta} = \dfrac{1}{2} i_m^2 g_{\theta m}^{\mathrm{I}} \end{cases} \tag{15}$$

$$\begin{cases} F_x^{\mathrm{II}} = \dfrac{1}{2} i_n^2 \dfrac{\mathrm{d}L(\theta, x, i_n)}{\mathrm{d}x} = \dfrac{1}{2} i_n^2 g_{xn}^{\mathrm{II}} \\ T_\theta^{\mathrm{II}} = \dfrac{1}{2} i_n^2 \dfrac{\mathrm{d}L(\theta, x, i_n)}{\mathrm{d}\theta} = \dfrac{1}{2} i_n^2 g_{\theta n}^{\mathrm{II}} \end{cases} \tag{16}$$

where m is one of the three phases from stator I and n is one of the three phases from stator II, respectively, where

$$g_{\theta m}^{\mathrm{I}} = \frac{\mathrm{d}L(\theta, x, i_m)}{\mathrm{d}\theta}, \quad g_{xm}^{\mathrm{I}} = \frac{\mathrm{d}L(\theta, x, i_m)}{\mathrm{d}x},$$
$$g_{\theta n}^{\mathrm{II}} = \frac{\mathrm{d}L(\theta, x, i_n)}{\mathrm{d}\theta} \text{ and } g_{xn}^{\mathrm{II}} = \frac{\mathrm{d}L(\theta, x, i_n)}{\mathrm{d}x}$$

The total force and torque generations of the RLSRM can be represented as

$$\begin{cases} F_x = F_x^{\mathrm{I}} + F_x^{\mathrm{II}} = \dfrac{1}{2} i_m^2 g_{xm}^{\mathrm{I}} + \dfrac{1}{2} i_n^2 g_{xn}^{\mathrm{II}} \\ T_\theta = T_\theta^{\mathrm{I}} + T_\theta^{\mathrm{II}} = \dfrac{1}{2} i_m^2 g_{\theta m}^{\mathrm{I}} + \dfrac{1}{2} i_n^2 g_{\theta n}^{\mathrm{II}} \end{cases} \tag{17}$$

From the above equations, the phase currents of stator I and stator II can be calculated as

$$\begin{cases} i_m = \sqrt{\dfrac{2T_\theta g_{xn}^{\mathrm{II}} - 2F_x g_{\theta n}^{\mathrm{II}}}{g_{\theta m}^{\mathrm{I}} g_{xn}^{\mathrm{II}} - g_{xm}^{\mathrm{I}} g_{\theta n}^{\mathrm{II}}}} \\ i_n = \sqrt{\dfrac{2F_x g_{\theta m}^{\mathrm{I}} - 2T_\theta g_{xm}^{\mathrm{I}}}{g_{\theta m}^{\mathrm{I}} g_{xn}^{\mathrm{II}} - g_{xm}^{\mathrm{I}} g_{\theta n}^{\mathrm{II}}}} \end{cases} \tag{18}$$

3.2 Finite element method (FEM) analysis

Fig. 2 shows the magnetic flux distribution at the position of $x = 0$ at $\theta = 20°$ with the current excitation of the level at 2 A. $x = 0$ mm stands for the exact middle position of the mover with respect to the two stators and $\theta = 0°$ is the fully aligned position from phase A of the two stators. It can be observed that there are two different kinds of flux which generate the propulsion force and the torque simultaneously. Since the magnetic paths for the force and the torque generation share the same flux lines, the axes of the linear and the rotary movement are highly coupled.

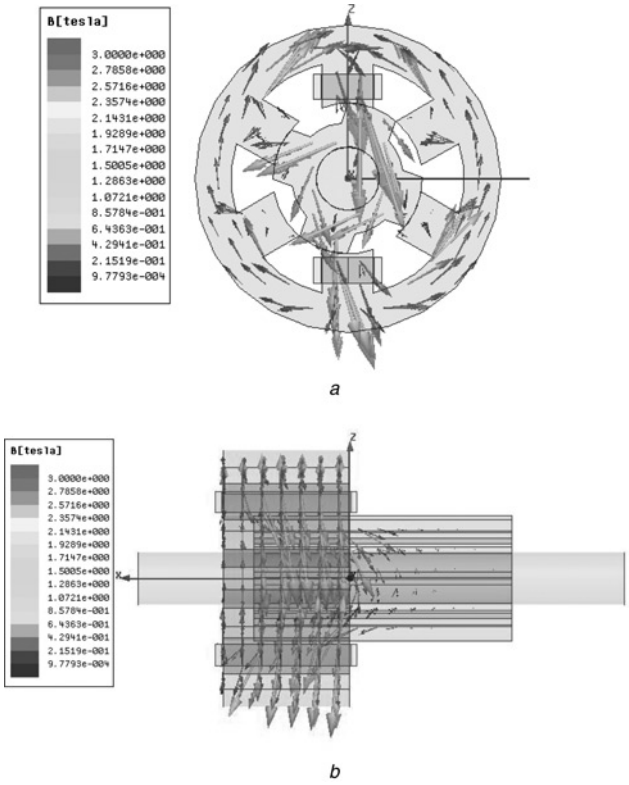

Fig. 2 *Flux distribution*
a Front view
b Side view

The flux-linkage of any one phase can be calculated and the contour according to different angular and linear positions at a current excitation of 2 A can be drawn as shown in Fig. 3*a*. Since the machine operates under the linear region, g_θ and g_x can be derived from the simulation results of the flux-linkage values. Torque output profiles according to different linear displacements can be derived as shown in Fig. 3*b*. It is clear that the torque is not only a function of the angular displacement, but it also depends on the linear position of the mover shaft. It can also be deduced from Fig. 3*c* of the force output profiles under different linear positions against the angular displacement that the force is the function of both the linear and the angular displacements. Therefore the linear and the rotary axes of motion are highly coupled.

3.3 Torque and force distribution function

From the above theoretical deductions and the simulation analysis, given any linear and angular position, the current of any phase from any stator contributes to a simultaneous force and torque generation. If $x = 0$ mm stands for the exact middle position with the mover with respect to the two stators, then the excitation phase(s) are different for the positive and the negative force commands though the absolute command value is the same. Meanwhile, for the different angular displacements, the torque generation corresponds to different phase(s) if $\theta = 0°$ stand for the fully

doi: 10.1049/iet-epa.2013.0248

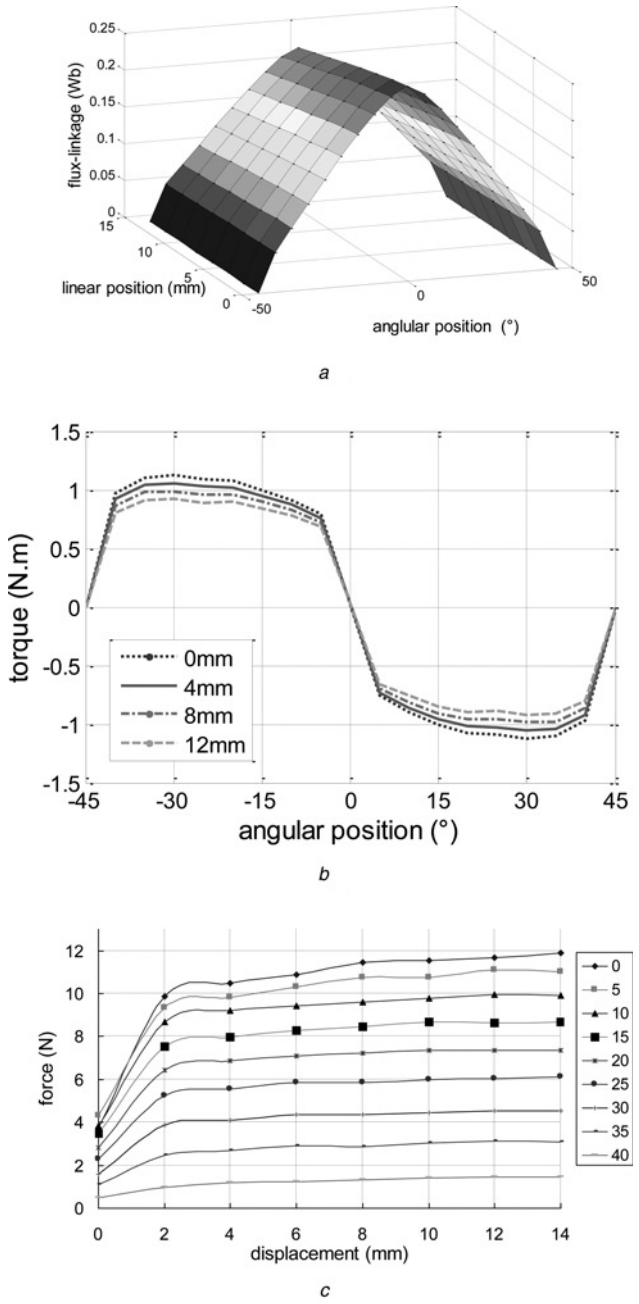

Fig. 3 *Electromagnetic characteristics*

a Flux-linkage characteristics
b Torque profiles
c Force profiles at 2 A

Table 2 Torque and force distribution function

Position x, mm	Angle θ	$T_\theta^* > 0$	$T_\theta^* < 0$
$0 \le x < 14$	$0° \le \theta < 10°$	$T_\theta = T_{\theta C}^{\mathrm{I}} + T_{\theta A}^{\mathrm{II}}$	$T_\theta = T_{\theta B}^{\mathrm{I}} + T_{\theta C}^{\mathrm{II}}$
	$10° \le \theta < 20°$	$F_x = F_{xC}^{\mathrm{I}} + F_{xA}^{\mathrm{II}}$ $T_\theta = T_{\theta C}^{\mathrm{I}} + T_{\theta A}^{\mathrm{II}}$	$F_x = F_{xB}^{\mathrm{I}} + F_{xC}^{\mathrm{II}}$ $T_\theta = T_{\theta A}^{\mathrm{I}} + T_{\theta C}^{\mathrm{II}}$
	$20° \le \theta < 30°$	$F_x = F_{xC}^{\mathrm{I}} + F_{xA}^{\mathrm{II}}$ $T_\theta = T_{\theta B}^{\mathrm{I}} + T_{\theta C}^{\mathrm{II}}$	$F_x = F_{xA}^{\mathrm{I}} + F_{xC}^{\mathrm{II}}$ $T_\theta = T_{\theta A}^{\mathrm{I}} + T_{\theta C}^{\mathrm{II}}$
	$30° \le \theta < 40°$	$F_x = F_{xB}^{\mathrm{I}} + F_{xC}^{\mathrm{II}}$ $T_\theta = T_{\theta B}^{\mathrm{I}} + T_{\theta C}^{\mathrm{II}}$	$F_x = F_{xA}^{\mathrm{I}} + F_{xC}^{\mathrm{II}}$ $T_\theta = T_{\theta A}^{\mathrm{I}} + T_{\theta B}^{\mathrm{II}}$
	$40° \le \theta < 50°$	$F_x = F_{xB}^{\mathrm{I}} + F_{xC}^{\mathrm{II}}$ $T_\theta = T_{\theta A}^{\mathrm{I}} + T_{\theta B}^{\mathrm{II}}$	$F_x = F_{xA}^{\mathrm{I}} + F_{xB}^{\mathrm{II}}$ $T_\theta = T_{\theta C}^{\mathrm{I}} + T_{\theta B}^{\mathrm{II}}$
	$50° \le \theta < 60°$	$F_x = F_{xA}^{\mathrm{I}} + F_{xB}^{\mathrm{II}}$ $T_\theta = T_{\theta A}^{\mathrm{I}} + T_{\theta B}^{\mathrm{II}}$	$F_x = F_{xC}^{\mathrm{I}} + F_{xB}^{\mathrm{II}}$ $T_\theta = T_{\theta C}^{\mathrm{I}} + T_{\theta A}^{\mathrm{II}}$
	$60° \le \theta < 70°$	$F_x = F_{xA}^{\mathrm{I}} + F_{xB}^{\mathrm{II}}$ $T_\theta = T_{\theta A}^{\mathrm{I}} + T_{\theta B}^{\mathrm{II}}$	$F_x = F_{xC}^{\mathrm{I}} + F_{xA}^{\mathrm{II}}$ $T_\theta = T_{\theta B}^{\mathrm{I}} + T_{\theta A}^{\mathrm{II}}$
	$70° \le \theta < 80°$	$F_x = F_{xA}^{\mathrm{I}} + F_{xB}^{\mathrm{II}}$ $T_\theta = T_{\theta C}^{\mathrm{I}} + T_{\theta A}^{\mathrm{II}}$	$F_x = F_{xB}^{\mathrm{I}} + F_{xA}^{\mathrm{II}}$ $T_\theta = T_{\theta B}^{\mathrm{I}} + T_{\theta A}^{\mathrm{II}}$
	$80° \le \theta < 90°$	$F_x = F_{xC}^{\mathrm{I}} + F_{xA}^{\mathrm{II}}$ $T_\theta = T_{\theta A}^{\mathrm{I}} + T_{\theta C}^{\mathrm{II}}$	$F_x = F_{xB}^{\mathrm{I}} + F_{xA}^{\mathrm{II}}$ $T_\theta = T_{\theta C}^{\mathrm{I}} + T_{\theta B}^{\mathrm{II}}$
$-14 \le x < 0$	$0° \le \theta < 10°$	$F_x = F_{xA}^{\mathrm{I}} + F_{xC}^{\mathrm{II}}$ $T_\theta = T_{\theta A}^{\mathrm{I}} + T_{\theta C}^{\mathrm{II}}$	$F_x = F_{xC}^{\mathrm{I}} + F_{xB}^{\mathrm{II}}$ $T_\theta = T_{\theta C}^{\mathrm{I}} + T_{\theta A}^{\mathrm{II}}$
	$10° \le \theta < 20°$	$F_x = F_{xA}^{\mathrm{I}} + F_{xC}^{\mathrm{II}}$ $T_\theta = T_{\theta C}^{\mathrm{I}} + T_{\theta B}^{\mathrm{II}}$	$F_x = F_{xC}^{\mathrm{I}} + F_{xA}^{\mathrm{II}}$ $T_\theta = T_{\theta C}^{\mathrm{I}} + T_{\theta A}^{\mathrm{II}}$
	$20° \le \theta < 30°$	$F_x = F_{xC}^{\mathrm{I}} + F_{xB}^{\mathrm{II}}$ $T_\theta = T_{\theta C}^{\mathrm{I}} + T_{\theta B}^{\mathrm{II}}$	$F_x = F_{xC}^{\mathrm{I}} + F_{xA}^{\mathrm{II}}$ $T_\theta = T_{\theta B}^{\mathrm{I}} + T_{\theta A}^{\mathrm{II}}$
	$30° \le \theta < 40°$	$F_x = F_{xC}^{\mathrm{I}} + F_{xB}^{\mathrm{II}}$ $T_\theta = T_{\theta C}^{\mathrm{I}} + T_{\theta B}^{\mathrm{II}}$	$F_x = F_{xB}^{\mathrm{I}} + F_{xA}^{\mathrm{II}}$ $T_\theta = T_{\theta C}^{\mathrm{I}} + T_{\theta B}^{\mathrm{II}}$
	$40° \le \theta < 50°$	$F_x = F_{xC}^{\mathrm{I}} + F_{xB}^{\mathrm{II}}$ $T_\theta = T_{\theta B}^{\mathrm{I}} + T_{\theta A}^{\mathrm{II}}$	$F_x = F_{xC}^{\mathrm{I}} + F_{xB}^{\mathrm{II}}$ $T_\theta = T_{\theta C}^{\mathrm{I}} + T_{\theta B}^{\mathrm{II}}$
	$50° \le \theta < 60°$	$F_x = F_{xB}^{\mathrm{I}} + F_{xA}^{\mathrm{II}}$ $T_\theta = T_{\theta B}^{\mathrm{I}} + T_{\theta A}^{\mathrm{II}}$	$F_x = F_{xC}^{\mathrm{I}} + F_{xB}^{\mathrm{II}}$ $T_\theta = T_{\theta A}^{\mathrm{I}} + T_{\theta C}^{\mathrm{II}}$
	$60° \le \theta < 70°$	$F_x = F_{xB}^{\mathrm{I}} + F_{xA}^{\mathrm{II}}$ $T_\theta = T_{\theta B}^{\mathrm{I}} + T_{\theta A}^{\mathrm{II}}$	$F_x = F_{xA}^{\mathrm{I}} + F_{xC}^{\mathrm{II}}$ $T_\theta = T_{\theta A}^{\mathrm{I}} + T_{\theta B}^{\mathrm{II}}$
	$70° \le \theta < 80°$	$F_x = F_{xB}^{\mathrm{I}} + F_{xA}^{\mathrm{II}}$ $T_\theta = T_{\theta A}^{\mathrm{I}} + T_{\theta C}^{\mathrm{II}}$	$F_x = F_{xA}^{\mathrm{I}} + F_{xB}^{\mathrm{II}}$ $T_\theta = T_{\theta A}^{\mathrm{I}} + T_{\theta B}^{\mathrm{II}}$
	$80° \le \theta < 90°$	$F_x = F_{xA}^{\mathrm{I}} + F_{xC}^{\mathrm{II}}$	$F_x = F_{xA}^{\mathrm{I}} + F_{xB}^{\mathrm{II}}$

aligned positions from phase A to the stator I or II. According to the machine topology, the excitation scheme can thus be tabulated as listed in Table 2. For any specific position and angular displacement, Table 2 shows which phases should be activated for a proper force and torque generation. For example, for the case of a positive displacement command and angular position between 10° and 20°, if a negative torque command is required, then phase A from stator I and phase C from stator II shall be activated at the same time. The current values of phases A and C can be solved according to (17) together with g_θ and g_x, which can be calculated according to the simulated flux-linkage profiles from the FEM. T_θ^* is the torque reference and it can be positive or negative. m stands for one of the three phases from the phases A, B or C of stator I and n is one of the three phases that can be A, B or C, respectively, from stator II. F_{xm}^{I}, F_{xn}^{II}, $T_{\theta m}^{\mathrm{I}}$ and $T_{\theta n}^{\mathrm{II}}$ are the generated force and torque from stators I and II, respectively.

The flowchart for the phase current derivation with the TFDF can be summarised as shown in Fig. 4. First, a single phase is attempted regarding the linear force command $F_x^{\mathrm{I}*}$ from stator I at a specific linear and angular position. Single phases A, B or C can be determined according to (9) then the value of i_m^* can be derived. The intermediate torque value $T_\theta^{\mathrm{I}'}$ can be calculated from the second equation of (9) and it is compared with the desired force command $T_\theta^{\mathrm{I}*}$. If they are not equal, the algorithm continues to consult Table 2 and solve the required i_m^* and i_n^* according to (18).

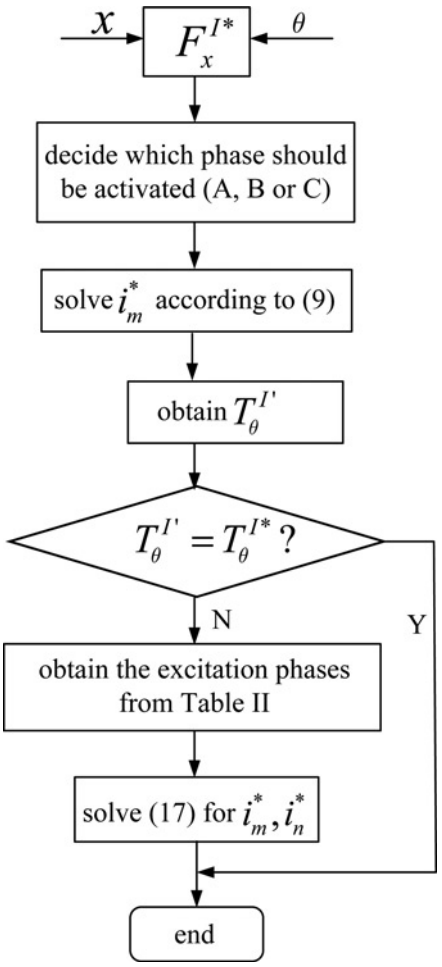

Fig. 4 *Flowchart of the current derivation with the TFDF*

4 Decoupling control of the RLSRM

4.1 Derivation of the phase current

From (6), the voltage equation of stator I and stator II can be given by

$$\begin{cases} u_m = R_m i_m + L(\theta, x, i_m)\dfrac{\mathrm{d}i_m}{\mathrm{d}t} + i_m g_{\theta m}^{\mathrm{I}} \omega_\theta + i_m g_{xm}^{\mathrm{I}} v_x \\ u_n = R_n i_n + L(\theta, x, i_n)\dfrac{\mathrm{d}i_n}{\mathrm{d}t} + i_n g_{\theta n}^{\mathrm{II}} \omega_\theta + i_n g_{xn}^{\mathrm{II}} v_x \end{cases} \tag{19}$$

where u_m and u_n are the applied voltage to the phase winding of stator I and stator II and R_m and R_n are the phase resistances of stator I and stator II, respectively. The above equation can be further represented as (see (20))

where $a_0 = (1/L(\theta, x, i_m))$, $a_1 = (R_m/L(\theta, x, i_m))$, $a_2 = (g_{\theta m}^{\mathrm{I}}/L(\theta, x, i_m))$, $a_3 = (g_{xm}^{\mathrm{I}}/L(\theta, x, i_m))$; $b_0 = (1/L(\theta, x, i_n))$, $b_1 = (R_n/L(\theta, x, i_n))$, $b_2 = (g_{\theta n}^{\mathrm{II}}/L(\theta, x, i_n))$ and $b_3 = (g_{xn}^{\mathrm{II}}/L(\theta, x, i_n))$.

The block diagram of the current controller for any one phase of the stator I can be derived as shown in Fig. 5.

4.2 Position controller design for the RLSRM

As denoted by (12), it is clear that the electromagnetic force and the torque generation can be indirectly controlled by the phase currents. The phase current is dependent not only on the angular and the linear speed, but is relevant to the phase inductance, which is a function with respect to the current and the mover position from both the linear and the rotary directions. Regardless of the load, (9) can be rewritten in the state-space form as

$$\boldsymbol{Y} = \boldsymbol{A}\ddot{\boldsymbol{U}} + \boldsymbol{B}\dot{\boldsymbol{U}} \tag{21}$$

where

$$Y = [F_x \quad T_\theta]^{\mathrm{T}}, \quad A = \begin{bmatrix} M & 0 \\ 0 & J \end{bmatrix},$$
$$B = \begin{bmatrix} D & 0 \\ 0 & K \end{bmatrix} \text{ and } \dot{U} = \begin{bmatrix} \dot{x} & \dot{\theta} \end{bmatrix}^{\mathrm{T}}$$

Therefore the open-loop transfer function for the RLSRM can be represented as

$$P(s) = \frac{K_p}{As^2 + Bs} \tag{22}$$

with $K_p = [1 \quad 1000]^{\mathbf{T}}$. The constant of 1000 is the unit conversion from millimeter to meter. A proportional–integral (PI) controller and a proportional–derivative (PD) controller are employed for the angular and the linear

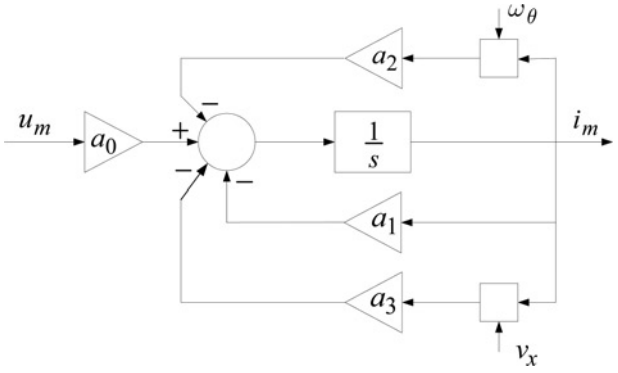

Fig. 5 *Block diagram of one phase of stator I*

$$\begin{cases} \dfrac{\mathrm{d}i_m}{\mathrm{d}t} = -\dfrac{R_m}{L(\theta, x, i_m)} i_m - \dfrac{g_{\theta m}^{\mathrm{I}}}{L(\theta, x, i_m)} \omega_\theta i_m - \dfrac{g_{xm}^{\mathrm{I}}}{L(\theta, x, i_m)} v_x i_m + \dfrac{u_m}{L(\theta, x, i_m)} \\ \qquad = -a_1 i_m - a_2 \omega_\theta i_m - a_3 v_x i_m + a_0 u_m \\ \dfrac{\mathrm{d}i_n}{\mathrm{d}t} = -\dfrac{R_n}{L(\theta, x, i_n)} i_n - \dfrac{g_{\theta n}^{\mathrm{II}}}{L(\theta, x, i_n)} \omega_\theta i_n - \dfrac{g_{xn}^{\mathrm{II}}}{L(\theta, x, i_n)} v_x i_n + \dfrac{u_n}{L(\theta, x, i_n)} \\ \qquad = -b_1 i_n - b_2 \omega_\theta i_n - b_3 v_x i_n + b_0 u_n \end{cases} \tag{20}$$

doi: 10.1049/iet-epa.2013.0248

position control, respectively, denoted as

$$\begin{cases} C_\theta(s) = K_{\theta\mathrm{P}} + \dfrac{K_{\theta\mathrm{I}}}{s} \\ C_x(s) = K_{x\mathrm{P}} + K_{x\mathrm{D}}s \end{cases} \tag{23}$$

where $K_{\theta\mathrm{P}}$, $K_{\theta\mathrm{I}}$ are the proportional and the integral gains of the angular position controller and $K_{x\mathrm{P}}$ and $K_{x\mathrm{D}}$ are the proportional and the derivative gains for the position controller, respectively. As shown in Fig. 6, the control system first receives the angular and the position commands $R_\theta(s)$ and $R_x(s)$, then the position controllers generate the corresponding torque and force commands T_θ^* and F_x^*, respectively. The transfer function $N(s)$ stands for the FTDF and the phase currents derivation of stator I and stator II based on (18), and it calculates the six phase current commands i_m^{I*} and i_n^{I*} for stator I and II, respectively, according to Fig. 4. $P(s)$ represents the transfer function of the RLSRM. It outputs the angular and the linear position information and the signals are fed back to the input of the position control system. The proposed position control scheme is illustrated in Fig. 7.

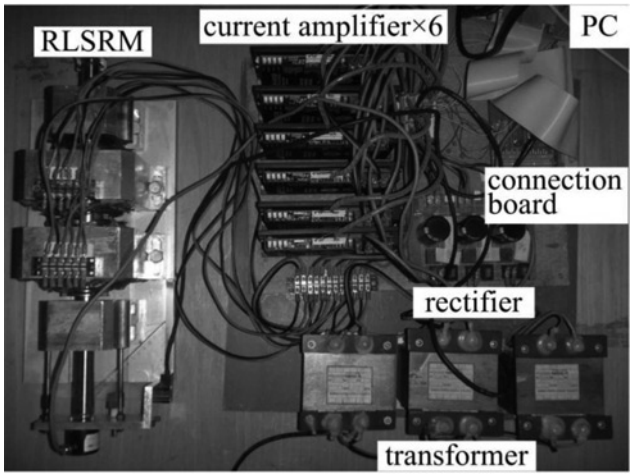

Fig. 8 *Experimental setup*

5 Experimental results

The experiment is performed on the dSPACE DS1104 controller platform which can directly interface with the real-time workshop of MATLAB/SIMULINK and the

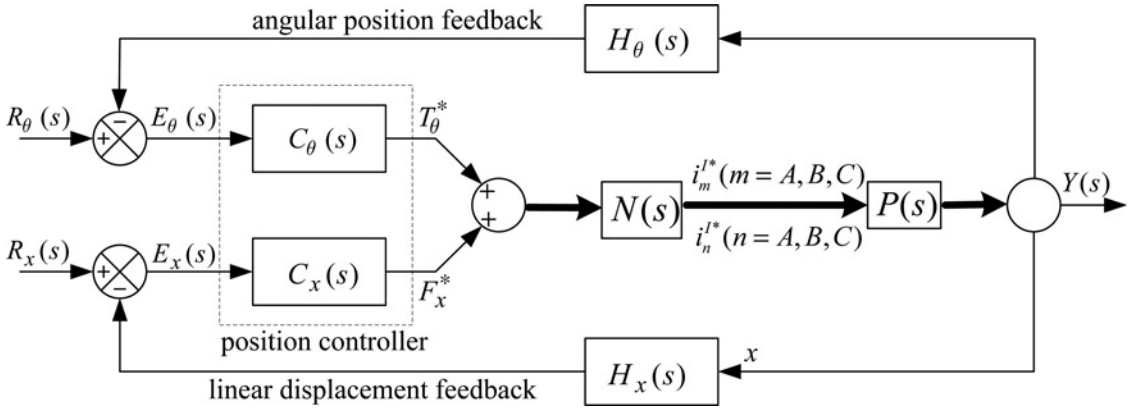

Fig. 6 *Block diagram of the position control loop*

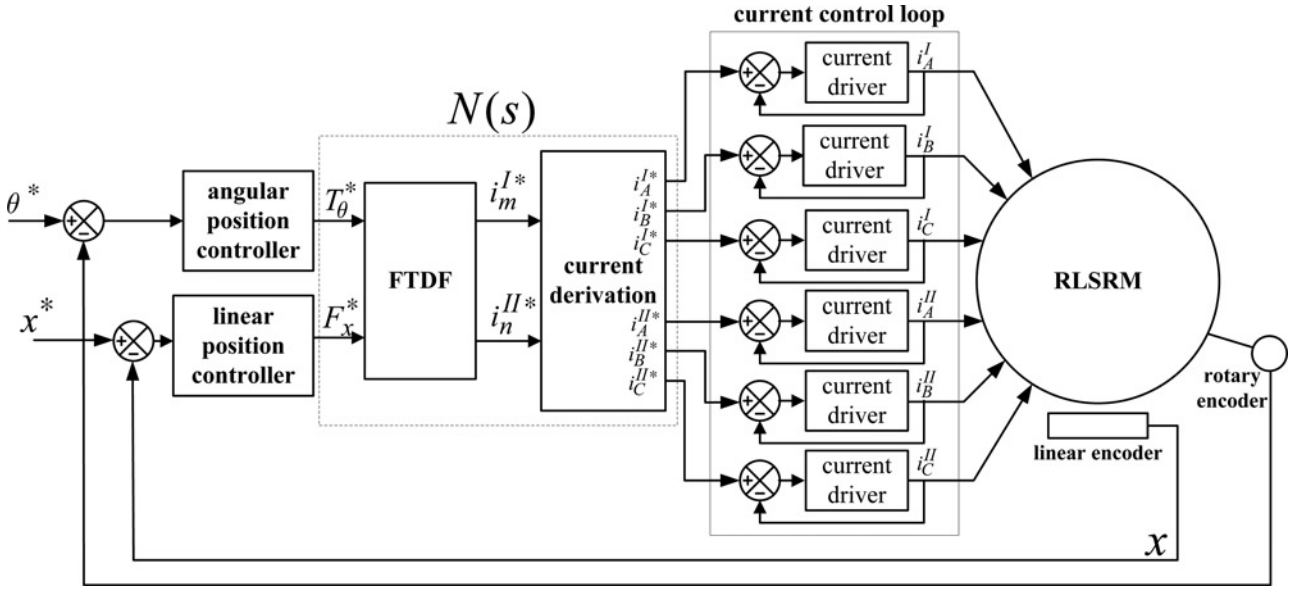

Fig. 7 *Control scheme*

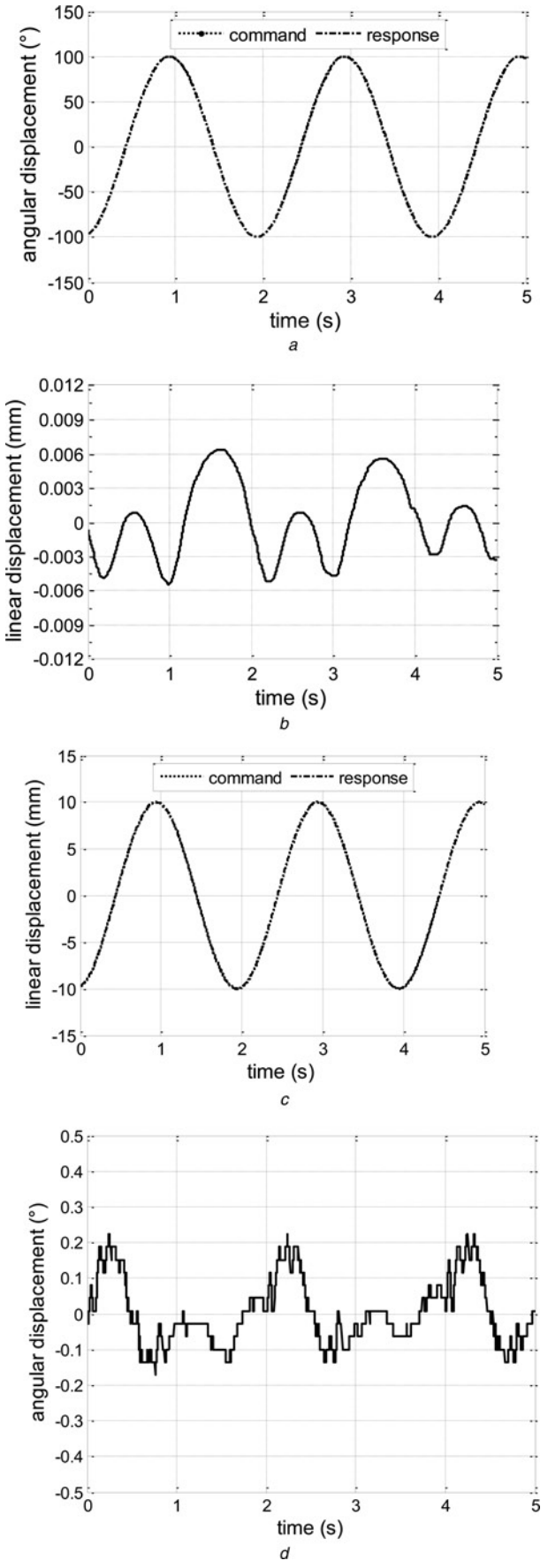

Fig. 9 *Decoupling test from each axis*

a Response profiles of the rotary direction
b Response profiles of the linear direction
c Response profiles of the linear direction
d Response profiles of the rotary direction

control parameters can be modified online. Six commercial amplifiers capable of an inner current regulation are employed with a 20 kHz switching frequency while the sampling rate of 1 kHz is selected for the position control loops. The rotary encoder with a resolution of 0.144° and the linear optical encoder with a resolution of 1 μm are mounted on the RLSRM and the overall experimental setup is shown in Fig. 8.

To test the decoupling effect from each axis of motion, the response profiles from a sinusoidal reference for each axis of motion can be found in Figs. 9*a* and *c*. Corresponding response waveforms from the other direction are provided, as shown in Figs. 9*b* and *d*. With the amplitude of the angular displacement of 200°, the dynamic position response from the linear motion falls into ±0.007 mm. Meanwhile, the dynamic angular displacement can be restricted to ±0.25° with a linear amplitude of 20 mm from the linear axis of motion. Therefore it can be concluded that the two axes of motion are successfully decoupled.

The parameters of the PI and the PD position controllers are regulated based on a trial and error basis [15] with the gains listed in Table 3. The results from the simulation and the experiment of the angular and the linear square response

Table 3 Controller parameters

	Angular position control loop		Linear position control loop	
gain	$K_{\theta P}$	$K_{\theta I}$	K_{xP}	K_{xD}
value	0.08	0.009	0.026	0.01495

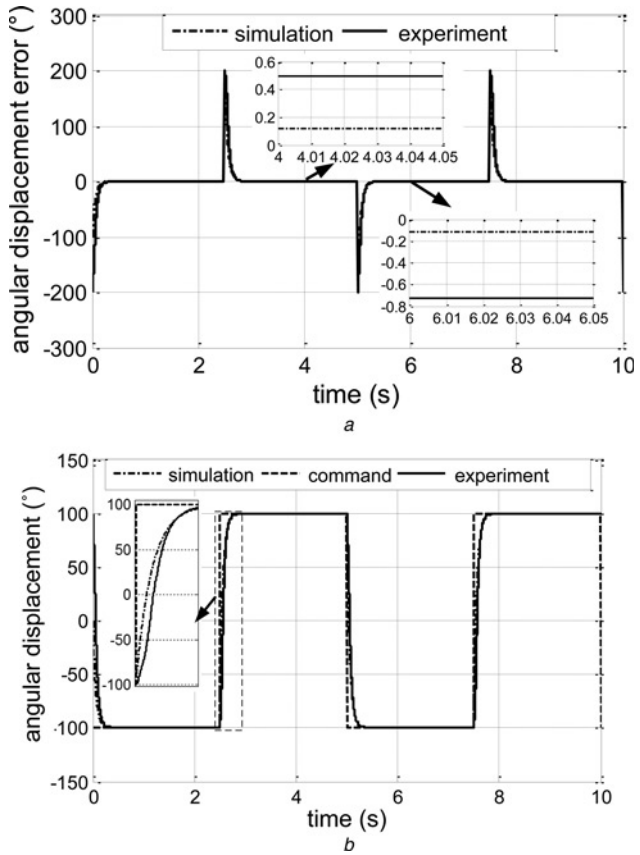

Fig. 10 *Response from the rotary axis*

a Dynamic error
b Trajectory response

doi: 10.1049/iet-epa.2013.0248

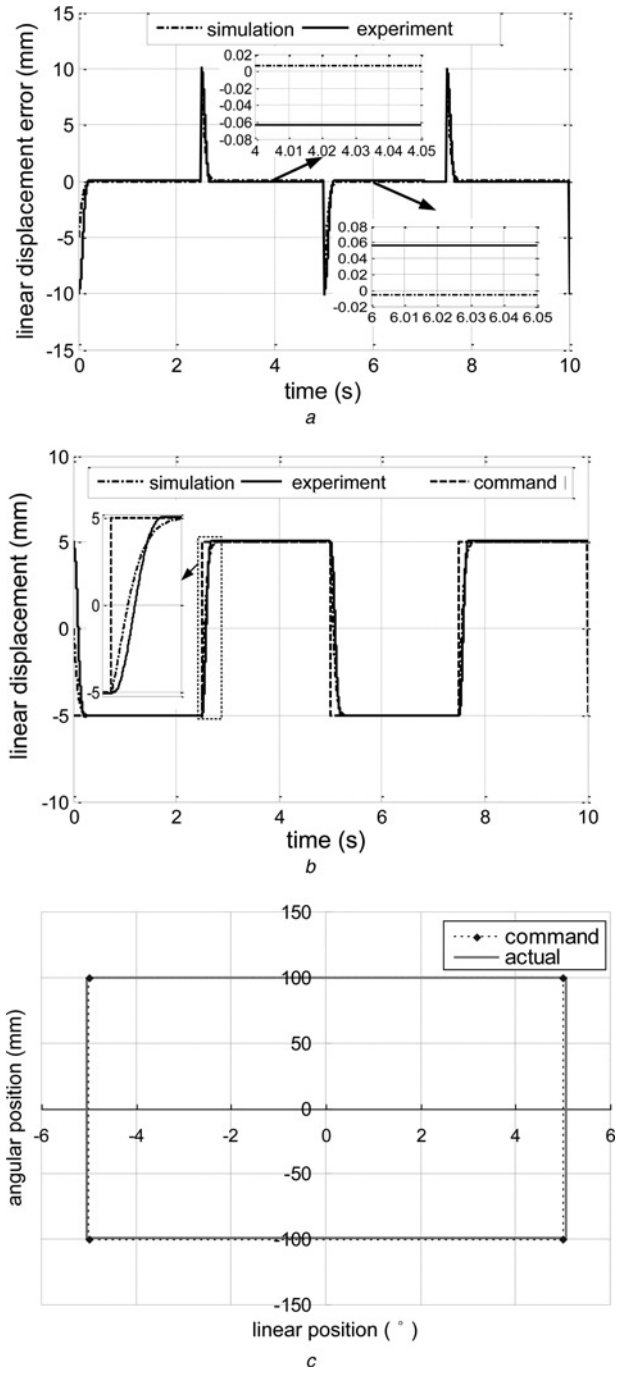

Fig. 11 *Response from the linear axis*

a Dynamic error
b Trajectory response
c Combined trajectory response

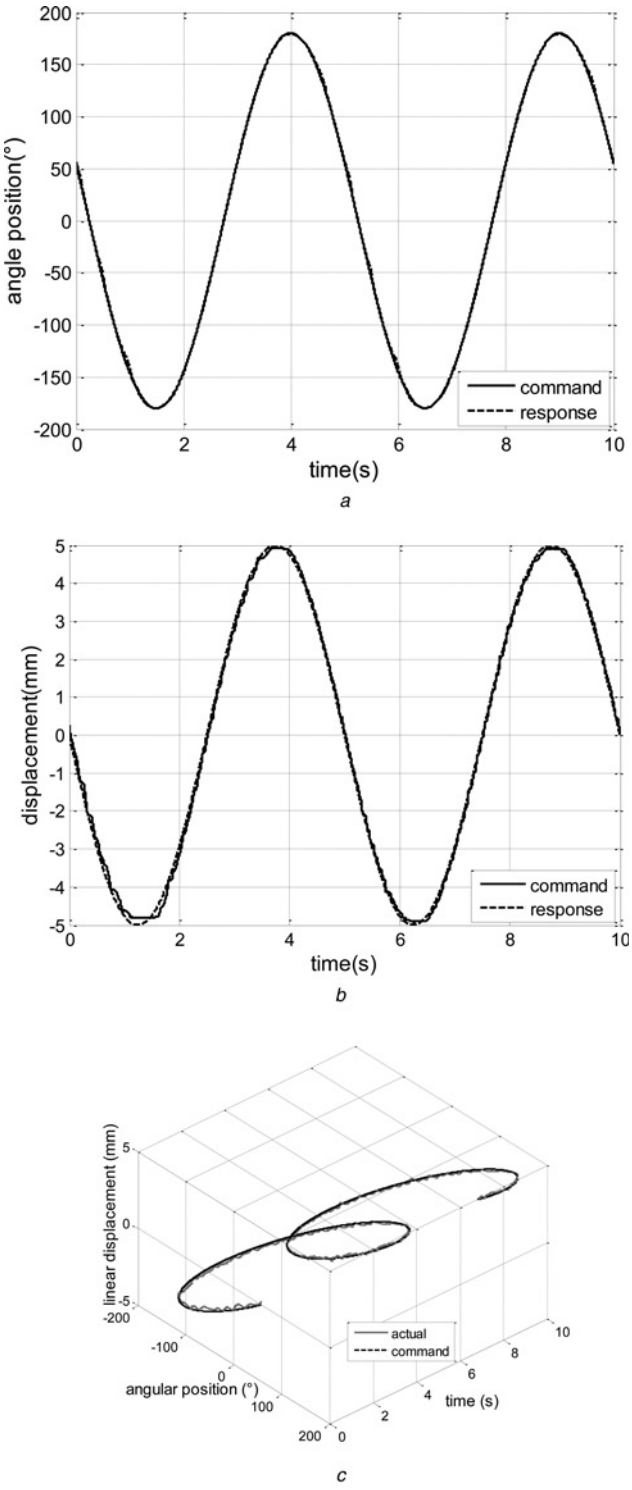

Fig. 12 *Sinusoidal position profiles from*

a The rotary axis
b The linear axis
c Combined trajectory response

profiles from the PI and the PD controllers can be found in Figs. 10 and 11, respectively. Both the overshoot-free position response waveforms can be enjoyed. With an amplitude of 200°, the absolute static errors of the experimental angular square position response fall into 0.482° and 0.564° for the positive and the negative transition and the simulation results of the absolute static errors of the angular square position response are equal to 0.120° for both the positive and the negative transition, respectively. For the response of the linear axis, the experimental static errors are within −0.063 and 0.056 mm for the positive and the negative transition and the simulation results of the static errors are equal to 0.006 mm for both the positive and the negative transition, respectively. Since there exist mechanical imperfections such as manufacture or assembly errors, the control performances from the simulation results are much better compared with that of the experiment. In addition, it is difficult to regulate the symmetric profiles from the positive and the negative transitions for both the axes of movement. If the square position commands from the linear and the rotary axes possess a half-period phase difference, the

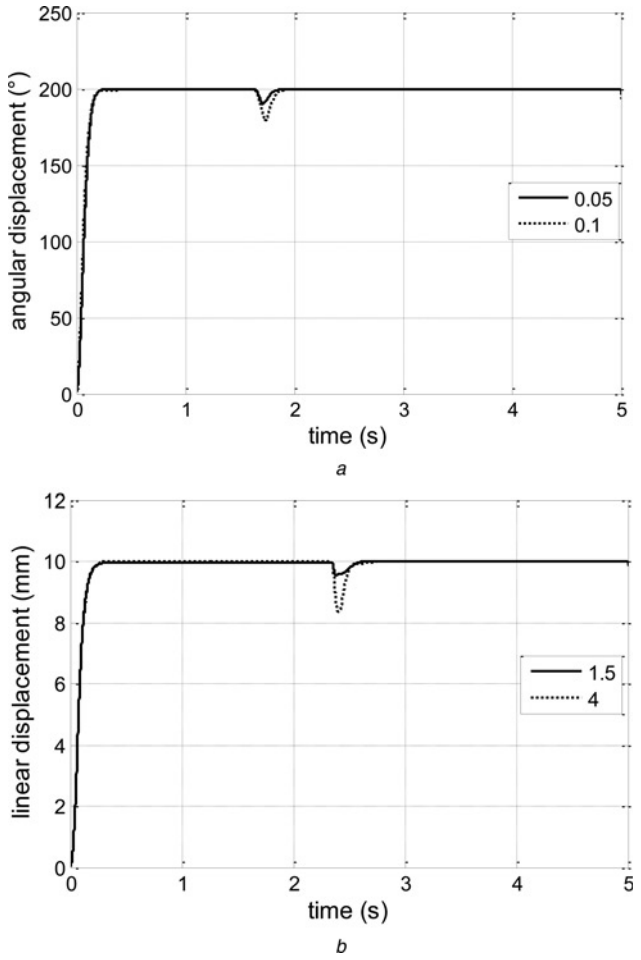

Fig. 13 *Step response with load disturbances from*
a Rotary
b Linear direction

composite graph of a triangular trajectory can be achieved, as shown in Fig. 11*c* for the dynamic response profiles.

The dynamic response profiles from the sinusoidal position commands can be found in Figs. 12*a* and *b* for the rotary and the linear axis, respectively. The performance from the rotary axis is better because of a lower inertia from this direction. If both the linear and the rotary axes follow the sinusoidal command with a period of 5 s, the dynamic response of a sinusoidal profile can be obtained as all the control parameters remain unchanged, as shown in Fig. 12*c*. The dynamic performance deteriorates according to the time-varying command signals since the control parameters are regulated based on a square response. However, the trajectory response demonstrates that the linear and the rotary axes are successfully decoupled and the position control from each axis of motion can be achieved independently.

To verify the disturbance rejection ability, load perturbations of 0.05, 0.1 N·m and 1.5, 4 N are added to the rotary and the linear axis of motion at 1.6 and 2.3 s, respectively, as shown in Fig. 13. Both the directions can regulate to their original steady-state profiles under a load interference. It can be concluded that both the axes of motion have a certain robustness.

6 Conclusion

A direct-drive RLSRM with inherently coupled axes of motion from the rotary and the linear movements is investigated. Based on the multiphase excitation method, a TFDF scheme is proposed for the RSLRM to decouple the two axes. The position controllers based on the simple PI and PD are constructed for the rotary and the linear axis, respectively. The simulation and the experimental results of the position response profiles from both the axes verify the effectiveness of the proposed TFDF that each axis of motion can be independently controlled simultaneously. Owing to the mechanical imperfections from the manufacturing and the assembly errors, the dynamic response profiles from the positive and the negative parts for the rotary and the linear axes of motion are not symmetric. It is suggested that more advanced control methodologies can be applied to the RLSRM for a uniform and high-precision position tracking performance for both the axes of motion based on the proposed TFDF.

7 Acknowledgments

The authors would like to thank the National Natural Science Foundation of China and the Guangdong Natural Science Foundation for sponsoring of the research projects under the codes 51007059, 51275312 and S2011010001208; the authors would also like to thank Shenzhen government fund JCYJ20130329144017199 for support.

8 References

1 Anorad Corp.: 'Rotary linear actuator'. U.S. Patent 6215 206, New York, USA, 4 October 2001
2 Krebs, G., Tounzi, A., Pauwels, B., Willemot, D., Piriou, F.: 'Modeling of a linear and rotary permanent magnet actuator', *IEEE Trans. Magn.*, 2008, **44**, (11), pp. 4357–4360, Part: 2
3 Ping, J., Heyun, L., Shuhua, F., Zhu, Z.Q., Huang, Y., Wang, X.: 'Analytical magnetic field analysis and prediction of cogging force and torque of a linear and rotary permanent magnet actuator', *IEEE Trans. Magn.*, 2011, **47**, (10), pp. 3004–3007
4 Ping, J., Heyun, L., Shuhua, F., Ho, S.L.: 'Decoupling control of linear and rotary permanent magnet actuator using two-directional d-q transformation', *IEEE Trans. Magn.*, 2012, **48**, (10), pp. 2585–2591
5 Bolognesi, P., Bruno, O., Papini, F., Biagini, V., Taponecco, L.: 'A low-complexity rotary-linear motor useable for actuation of active wheels'. Int. Symp. on Power Electronics Electrical Drives Automation and Motion (SPEEDAM), 2010, pp. 331–338
6 Bolognesi, P.: 'Structure and theoretical analysis of a novel rotary-linear isotropic brushless machine'. XIX Int. Conf. on Electrical Machines (ICEM), 2010, pp. 1–6
7 Bolognesi, P., Biagini, V.: 'Modeling and control of a rotary-linear drive using a novel isotropic brushless machine'. XIX Int. Conf. on Electrical Machines (ICEM), 2010, pp. 1–6
8 Pan, J.F., Yu, Z., Guangzhong, C.: 'Adaptive controller for the double-sided linear switched reluctance motor based on the nonlinear inductance modelling', *IET Electr. Power Appl.*, 2013, **7**, (1), pp. 1–15
9 Pan, J.F., Cheung, N.C., Guangzhong, C.: 'A rotary-linear switched reluctance motor'. Proc. Third Int. Conf. on Power Electronics Systems and Applications, 2009, pp. 1–4
10 Bentia, I., Szabo, L., Ruba, M.: 'On a rotary-linear switched reluctance motor'. Int. Symp. on Power Electronics, Electrical Drives, Automation and Motion (SPEEDAM), 2012, pp. 507–510
11 Bentia, I., Ruba, M., Szabo, L.: 'On the control of a rotary-linear switched reluctance motor'. Proc. Fifth Int. Symp. on Computational Intelligence and Intelligent Informatics (ISCIII), 2011, pp. 41–46
12 Pan, J.F., Cheung, N.C., Guangzhong, C.: 'Investigation of a rotary-linear switched reluctance motor'. XIX Int. Conf. on Electrical Machines (ICEM), 2010, pp. 1–4
13 Sato, Y.: 'Development of a 2-degree-of-freedom rotational/linear switched reluctance motor', *IEEE Trans. Magn.*, 2007, **43**, (6), pp. 2564–2566
14 Krishnan, R.: 'Switched reluctance motor drives: modeling, simulation, analysis, design, and applications' (CRC Press, Boca Raton, 2001)
15 Antonio, V.: 'Practical PID control' (Springer-Verlag, USA, 2006)

doi: 10.1049/iet-epa.2013.0248